ANL-77-9

PHYSICS OF REACTOR SAFETY

Quarterly Report
July–September 1976

ARGONNE NATIONAL LABORATORY, ARGONNE, ILLINOIS

Prepared for the U. S. NUCLEAR REGULATORY COMMISSION

The facilities of Argonne National Laboratory are owned by the United States Government. Under the terms of a contract (W-31-109-Eng-38) between the U. S. Energy Research and Development Administration, Argonne Universities Association and The University of Chicago, the University employs the staff and operates the Laboratory in accordance with policies and programs formulated, approved and reviewed by the Association.

MEMBERS OF ARGONNE UNIVERSITIES ASSOCIATION

The University of Arizona
Carnegie-Mellon University
Case Western Reserve University
The University of Chicago
University of Cincinnati
Illinois Institute of Technology
University of Illinois
Indiana University
Iowa State University
The University of Iowa
Kansas State University
The University of Kansas
Loyola University
Marquette University
Michigan State University
The University of Michigan
University of Minnesota
University of Missouri
Northwestern University
University of Notre Dame
The Ohio State University
Ohio University
The Pennsylvania State University
Purdue University
Saint Louis University
Southern Illinois University
The University of Texas at Austin
Washington University
Wayne State University
The University of Wisconsin

Printed in the United States of America
Available from
National Technical Information Service
U. S. Department of Commerce
5285 Port Royal Road
Springfield, Virginia 22161
Price: Printed Copy $3.50; Microfiche $3.00

Distribution Category:
Advanced Reactor Safety
Research—Fast Reactor
(NRC-7)

ANL-77-9

ARGONNE NATIONAL LABORATORY
9700 South Cass Avenue
Argonne, Illinois 60439

PHYSICS OF REACTOR SAFETY

Quarterly Report
July—September 1976

Applied Physics Division

December 1976

Work performed for the
Division of Reactor Safety Research
U. S. Nuclear Regulatory Commission

Previous reports in this series

ANL-76-6	July—September 1975
ANL-76-13	October—December 1975
ANL-76-72	January—March 1976
ANL-76-114	April—June 1976

TABLE OF CONTENTS

LIST OF TABLES

LIST OF FIGURES

PHYSICS OF REACTOR SAFETY

Quarterly Report
July-September 1976

I. ABSTRACT

This quarterly progress report summarizes work done in Argonne National Laboratory's Applied Physics Division and Components Technology Division for the Division of Reactor Safety Research of the U. S. Nuclear Regulatory Commission during the months of July-September 1976. The work in the Applied Physics Division includes reports on reactor safety research and technical coordination of the RSR safety analysis program by members of the Reactor Safety Appraisals Group, Monte Carlo analysis of safety-related critical assembly experiments by members of the Theoretical Fast Reactor Physics Group, and planning of DEMO safety-related critical experiments by members of the Zero Power Reactor (ZPR) Planning and Experiments Group. Work on reactor core thermal-hydraulic performed in the Components Technology Division is also included in this report.

TECHNICAL COORDINATION - FAST REACTOR SAFETY ANALYSIS (A2015)

II. SUMMARY

Further pipe rupture studies for the CRBR have been carried out using the DEMO and SAS codes with corrected input parameters in DEMO. General trends in the results are similar to those observed previously.

The reactivity calculations in the CLAZAS (clad motion) module of the SAS code have been checked and found accurate to about 10%.

The effect of using isotopic fission and capture energies rather than a lumped total energy per fission on subassembly power factors in the CRBR has been evaluated. It was concluded that differences in core subassembly power factors between those calculated by us and those in the CRBR PSAR are not due to the above effect but to reasons given previously. For the radial blanket the effect of using isotopic energies of fission and capture on subassembly power factors is larger, but this connot be evaluated as a cause of differences between our calculations and those in the CRBR PSAR because of the inconsistent burnup pattern assumed in the PSAR.

Major revisions were accomplished in the hydrodynamics routines in POOL to deal with the continuing problems caused by the development of incompressible regions. These include, a Distributed Particle-in-Cell technique in which the mass of a particle is distributed over a localized volume and energy was implemented; an approximate technique of decoupling the axial and radial motions for incompressible cells is being examined.

An improved point kinetics scheme in FX2 better able to deal with gross material motions is being developed. In this scheme the reactivity rather than the flux is extrapolated to predict future behavior.

Several additional improvements have been made in EPIC. Parameter studies and additional comparisons with PLUTO are under way.

The KACHINA code has been implemented on the IBM 370 195.

III. STUDY OF BASIC PROBLEMS IN ACCIDENT ANALYSIS

A. Initiating Condition Variations

1. Pipe Rupture Studies for the CRBR Using DEMO and SAS (H. H. Hummel and Kalimullah)

The calculations reported in the January-March Physics of Reactor Quarterly Report, ANL-76-72, have been redone to correct an inconsistency in the input parameters. The results are qualitatively similar to the previous ones. The minimum in the coolant flow through for a double-ended rupture at the CRBR inlet nozzle is now found to be 26% of the original value, in agreement with other calculations.[1,2] A revised parametric study of maximum coolant temperature vs. pin power, initial flow rate, and gap conductance is presented in Fig. 1. A revised comparison between DEMO and SAS calculations is presented in Table I. The DEMO3 model[2] uses updated input parameters for the CRBR as explained in Ref. 2. Further details of these calculations may be found in Ref. 3.

2. Clad Motion Reactivity Calculation by the CLAZAS Routine of the SAS Code (Kalimullah)

Because of preliminary results (later found incorrect) showing significant differences in feedback calculations between the SAS[4] and FX2[5] codes, the clad motion reactivity calculation in the CLAZAS routine of the SAS code was checked by a hand calculation for one case using the "Explicit Clad Motion Edit" printed out by the routine and equal parts and the worths of these parts were evaluated by linear interpolation as done in the CLAZAS routine. The had calculation gave a net clad worth of 22¢ compared to 20¢ calculated by the routine. In other hand calculations[6] similar underestimates of about 10% by the CLAZAS routine, have been found. In view of the approximations made in calculating the motion of the clad itself in the CLAZAS routine, this error of 10% in calculating the worth of the redistributed clad is not of much concern. Of course, when an improved model of treating the motion of the clad becomes available, this underestimate will become significant enough to correct.

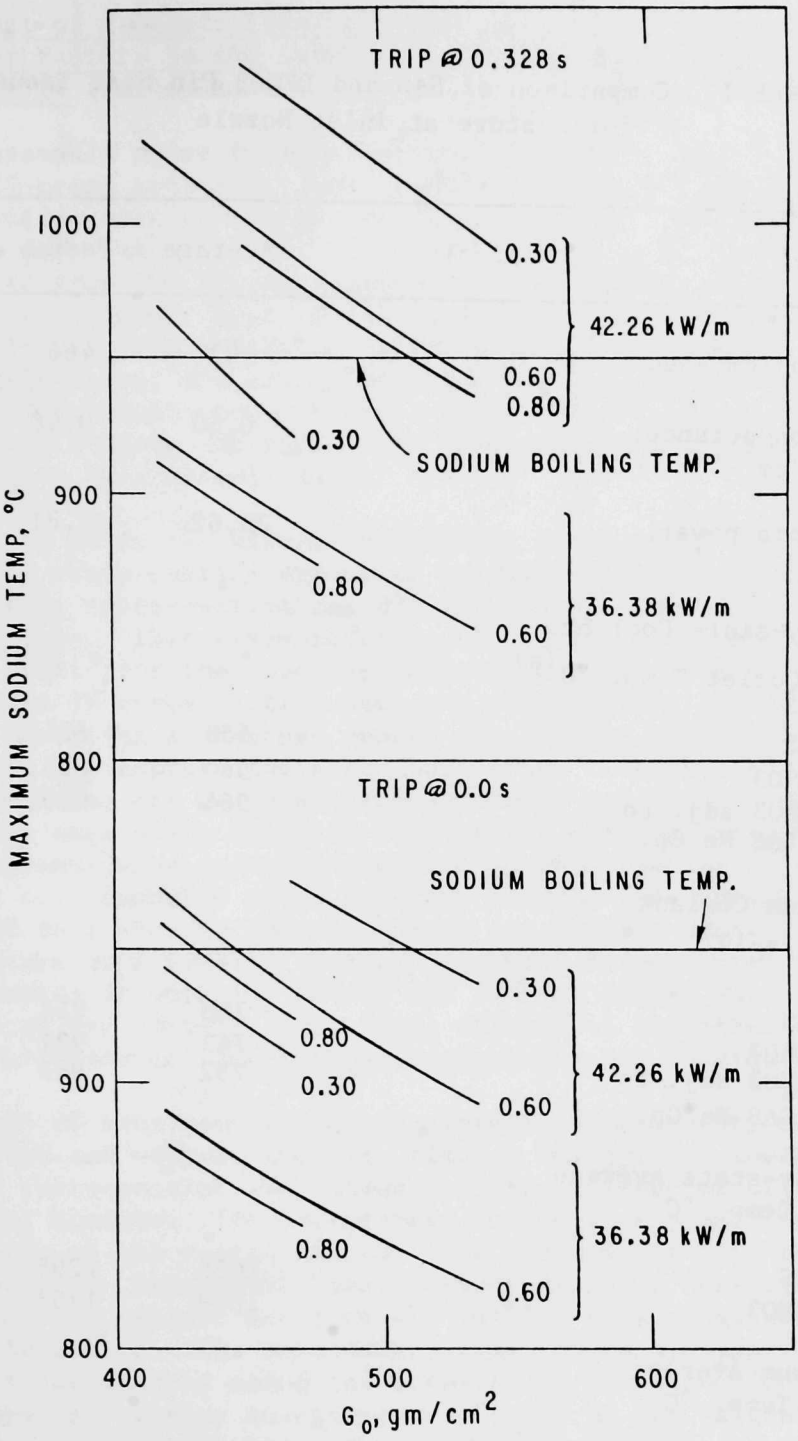

Fig. 1. Maximum Coolant Temperature Obtained for a Double-Ended Rupture at the Inlet Nozzle for Various Maximum Pin Power Densities, Fuel-Clad Gap Conductances (watts/cm^2-°C) and Coolant Mass Velocities G_0. The higher and lower pin power densities correspond to DEMO hot and peak channels. G_0 is 418, 466 and 487 gm/cm^2-sec for hot, peak, and average channels respectively.

TABLE I. Comparison of SAS and DEMO3 Pin Heat Transfer for Rupture at inlet Nozzle

Channel	Average	Peak	Hot
G_o, gms/cm^2-sec	487	466	418
Gap conductance, watts/cm^2-°C	0.60	0.60	0.45
Peak pin power, kw/m	25.62	34.81	40.42
Steady-state Coolant Core Outlet Temp, °C[(a)]			
SAS	558	625	692
DEMO3	560	625	690
DEMO3 adj. to SAS Na Cp.	564	630	699
Maximum Coolant Temp. °C[(a)]			
SAS	768	914	1052
DEMO3	743	931	1085
DEMO3 adj. to SAS Na Cp.	752	945	1079
Steady-state Average Fuel Temp, °C			
SAS	1028	1295	1568
DEMO3	1059	1353	1751
Maximum Average Fuel Temp. °C			
SAS	1064	1342	1613
DEMO3	1093	1397	1800

(a) Coolant inlet temperature 399°C. Boiling at 950°C suppressed.

3. Effect of Isotopic Fission and Capture Energies on Subassembly Power Factors in the CRBR at the Beginning of Equilibrium Cycle 14 (Kalimullah)

The subassembly power factors reported in Ref. 7 were calculated using our standard 27-group cross-sections based on ENDF/B Version III data with an isotope-independent average energy per fission event. Isotopic fission and capture energy data was not used. Core subassembly power factors were reported to differ from the values reported in the PSAR[8] Fig. 4.3-7 by up to 3.2% higher to 4.5% lower, most of the larger differences being in the outer core subassemblies. With a view to investigate the reasons for these rather significant differences, the effect of using isotopic fission and capture energy data on subassembly power factors was analyzed. Figure 2 shows the subassembly power factors and Fig. 3 the subassembly peak-to-average power density ratios for this calculation.

In order to study the effect of isotopic fission and capture energies, another 27-group cross-section set based on ENDF/B Version IV data was used because the former cross-section set did not contain isotopic fission and capture energy data. This cross-section set was also generated using the MC^2-2 and SDX codes[9] for the specific composition and geometry of the CRBR. Using the Version IV cross-section set, two calculations of radial power distribution, one using an average energy per fission event and the other with isotopic fission and capture energies, were done. Figure 4 shows the subassembly power factors using an average energy per fission event, and Fig. 5 shows the same using isotopic fission and capture energies. Figure 6 shows the subassemblywise radially-averaged power densities at the midheight of the reactor core computed using isotopic fission and capture energies. It should be noted that when an average energy per fission event is used the energy per capture in a fissile isotope can still be accounted for in the analysis by lumping it with the energy per fission event. What is not accounted for is the energy per capture in coolant, structural and other isotopes, and the isotopic variation of energies per capture and per fission.

Comparison of subassembly peak-to-average power density ratios between calculations with and without isotopic fission and capture energies (done with the Version IV cross-section set) shows largest differences of about 4% in row 10 of the radial blanket. The differences in row 11 are smaller and those in the outermost row of the radial blanket (row 12) are not more than about two tenths of a percent. Subassembly peak-to-average power density ratios with isotopic fission and capture energies are smaller than those without, in row 10 and larger in row 12. The subassembly peak-to-average power density ratios shown in Fig. 3 (calculated using the Version III cross-section set without isotopic fission and capture energies) are closer to the values obtained using the Version IV cross-section set without isotopic fission and capture energies than those with, the values in Fig. 3 being not more than a percent larger than the former values in row 10 of the radial blanket. In the core region the subassembly peak-to-average power density ratios obtained from all these three calculations differ only slightly by not more than a couple of tenths of a percent.

Core subassembly power factors calculated using the Version IV cross-section set with isotopic fission and capture energies, shown in Fig. 5 are up to 0.9% higher and up to 0.7% lower than those computed using the same

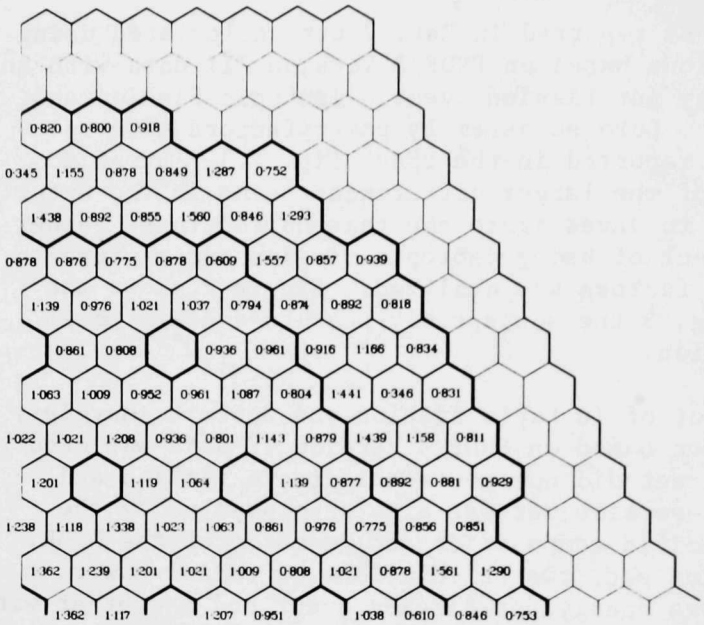

Fig. 2

Subassembly Power Factors for the LWR-Grade Plutonium Fueled Clinch River Breeder Reactor at the Beginning of Equilibrium Cycle 14.

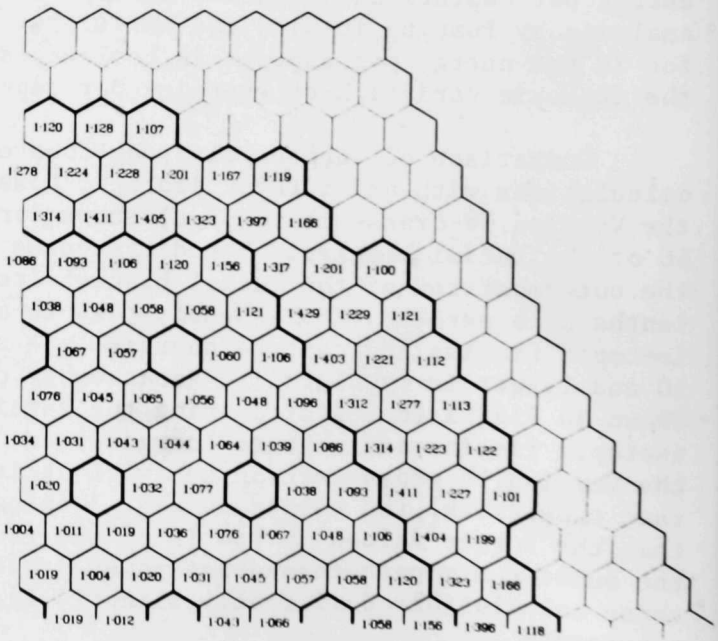

Fig. 3

Subassembly Peak-to-Average Power Density Ratios for the LWR-Grade Plutonium Fueled Clinch River Breeder Reactor at the Beginning of Equilibrium.

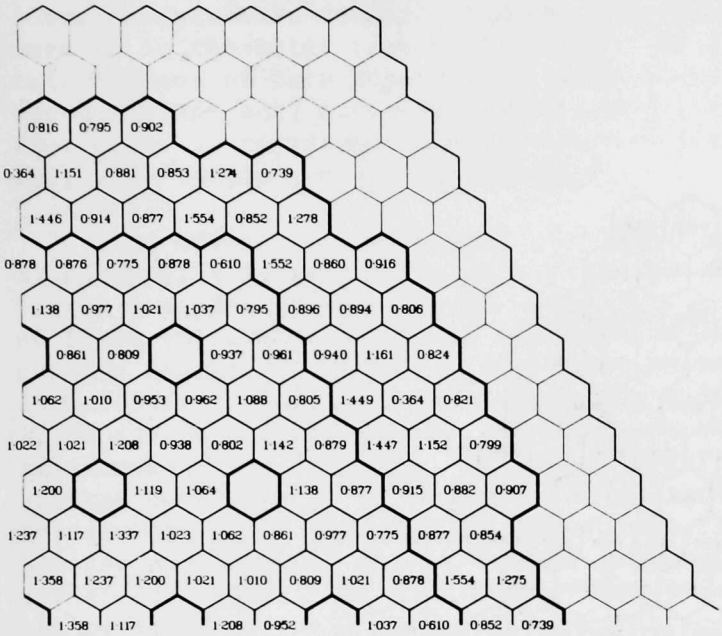

Fig. 4

Subassembly Power Factors for the LWR-Grade Plutonium Fueled Clinch River Breeder Reactor at the Beginning of Equilibrium Cycle 14 Without Capture Energy with an Average Energy/Fission.

Fig. 5

Subassembly Power Factors for the LWR-Grade Plutonium Fueled Clinch River Breeder Reactor at the Beginning of Equilibrium Cycle 14 with Isotopic Capture and Fission Energies.

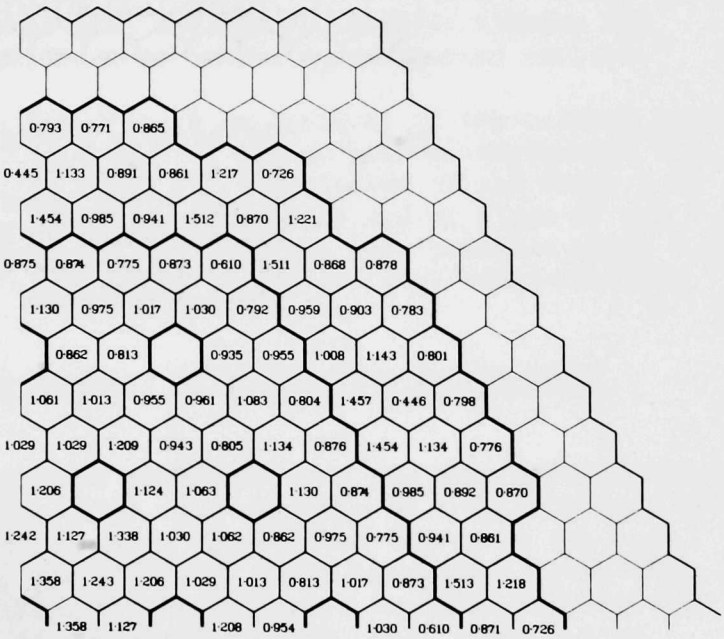

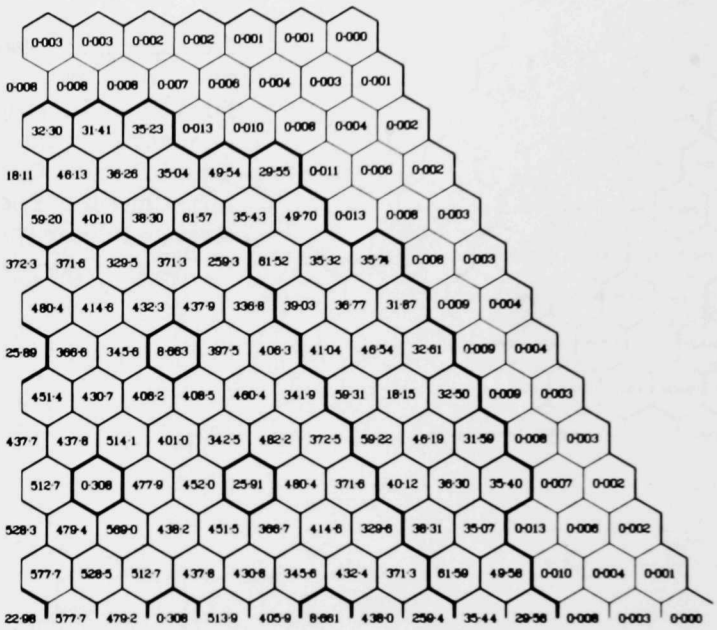

Fig. 6. Subassembly Average Power Densities for the LWR-Grade Plutonium Fueled Clinch River Breeder Reactor at the Beginning of Equilibrium Cycle 14 with Isotopic Capture and Fission Energies.

cross-section set with an average energy per fission event, shown in Fig. 4. Subassembly power factors calculated with isotopic fission and capture energies are higher in the inner core region and lower in the outer core region than those computed without. Comparison of Figs. 4 and 5 also shows the trend that fresher subassemblies in the core tend to have smaller power factors when isotopic fission and capture energies are accounted for, more so in the outer rows of the core. As far as the comparison of these two calculations of core subassembly power factors (using the Version IV cross-section set) shown in Figs. 4 and 5 with the values reported in the PSAR[8] Fig. 4.3-7 is concerned, the differences are larger for the computation with isotopic fission and capture energies.

The effect of considering isotopic fission and capture energies is significantly larger in the radial blanket because the capture power is a larger fraction of the fission power in the radial blanket. The power factors of fresh subassemblies of row 10 increase by up to 7.7% due to the additional capture energy. Strikingly, the power factor of the fresh subassembly identifications no. 51 in row 11 of the radial blanket increases by about 22.5% due to its low fission power (compared to other radial blanket subassemblies). The power factors of highlyburnt subassemblies in the radial blanket decreases by up to 4.5%. It is irrelevant to compare radial blanket subassembly power factors with the values reported in the PSAR Fig. 4.3-7 because an incorrect radial blanket subassembly-burnup pattern, different from any of the six blanket subassembly-burnup pattern, different from any of the six patterns it takes during its equilibrium operation, was used for the calculation of power factors reported in the PSAR.

This analysis indicates that the main reasons for the differences in the core subassembly power factors between our calculation reported earlier[7] and the PSAR Fig. 4.3-7 is not connected with the use of isotopic fission and capture energies, but are still believed to be the ones reported earlier.[7]

It is interesting to obtain from Fig. 6 an estimate of the capture power in control subassemblies. The central control rod of natural enrichment B_4C, inserted 2/3 into the core, produces about 4% of the power of the fresh fuel subassembly in row 2 of the core. Each control rod at rod at flats of row 7 containing 50% enriched B_4C and inserted 2/3 into the core produces about 7.6% of the power of the adjacent two cycle-burnt inner core fuel subassembly in the same row.

4. Modification of Flux-to-Pressure Trip Criterion in the DEMO2 Code (Kalimullah)

A double precision IBM version of the DEMO2 code was made operational at ANL earlier. Recently the flux-to-square root of pressure trip criterion was modified to a slightly more general form in the Fortran source of the code. Some unidentified errors exist in the automatic double precision conversion and optimization level 2 capabilities of the Fortran H Extended Compiler at ANL, so that the complete source of the modified DEMO2 code could not be compiled to make a double precision load module. For the time being, a modified double precision load module has been made by replacing only the subroutine PROTSYS (which contained all the modifications) in the old load module, and the resulting load module seems to work satisfactorily. Of course, the subroutine PROTSYS had to be compiled using our Fortran H Extended

Compiler which has some bugs. The resolution of these compiler bugs is being made by the Applied Mathematics Division.

5. Effect of the Use of ENDF/B-IV Data on the Computation of Sodium Void Worth in CRBR (P. H. Kier)

Reactivity coefficients for the Clinch River Breeder Reactor (CRBR) at end of equiliburium cycle (EOEC) conditions have been computed using two cross section libraries. One library was generated with use of ENDF/B-III data and the standard SDX/MC^2-2 procedure; the other library was generated with use of ENDF/B-IV data and SDX/MC^2-2 used in a mode that yielded refinements in the computation of resonance absorption and resonance scattering. Although computed Doppler coefficients and fuel worths were insensitive to differences in these cross section libraries, sodium void worths were quite sensitive to these differences. Sodium void worths were longer by 15% in the inner core and 33% overall when computed with the ENDF/B-IV library.

A study using perturbation theory calculations was made to determine for which isotopes the cross section differences lead to these differences in sodium void worth. Sodium void worths are obtained from perturbations in which sodium is removed from compositions and in which cross sections generated for unit cells in which sodium was absent. Proliminary calculations indicated that the effect on the sodium void worth of changing from ENDF/B-III to ENDF/B-III cross sections for an isotope is predicted poorly if the perturbation were performed without accounting for the effect on the real and the adjoint flux distributions of the change to ENDF/B-IV data for the isotope.

We considered the effect on the sodium void worth in the inner core of CRBR of replacing ENDF/B-III cross sections with ENDF/B-IV cross sections for 13 isotopes. A one-dimensional model was used in which the radial configuration at EOEC was the same as in the r-z model. The transverse height was adjusted such that the system was just critical when ENDF/B-III cross sections were used for all isotopes. Thirteen first-order perturbation theory problems were run, one for each isotope considered. For each problem, the real and adjoint flux distributions were computed with compositions having isotopes with ENDF/B-III cross sections except for the specified isotope in the inner core compositions, which had ENDF/B-IV cross sections. The sodium void perturbation was then performed.

Table II gives the results of the caluculations in terms of the percentage change in the sodium void worth arising from using ENDF/B-IV data for the isotope. Since the calculations were one-dimensional, the inner core implicitly extended to the extrapolated height of the reactor, the transverse leakage component of reactivity is overestimated significantly.

In the r-z calculation the magnitude of the leakage component of reactivity was about 40% of the total reactivity effect whereas in these calculations the leakage component was twice the total reactivity effect. Therefore the percentage differences given in the table exclude the leakage component and should be slightly small. However, as the primary purpose of this study is to compare the effect from different isotopes it is not important that the magnitude of the effect in each be slightly small. From the

table it is seen that the change in the sodium void worth arises principally from differences in the cross sections of the three heavy isotopes with the greatest atom densities: ^{238}U, ^{239}Pu, and ^{240}Pu.

TABLE II. Percentage Change in the Sodium Void Worth in the Inner Core of CRBR at EOEC in Changing from ENDF/B-III Data to ENDF/B-IV Data for Selected Isotopes

Isotope	% Change
^{235}U	0.25
^{238}U	4.91
^{239}Pu	2.23
^{240}Pu	2.85
^{241}Pu	-0.48
^{242}Pu	0.01
^{16}O	-0.16
Na	-0.13
Fe	0.68
Cr	-0.46
Ni	0.34
Mo	-0.74
Mn	0.39
Sum	9.69

B. Model Studies

1. Recriticality Studies (P. B. Abramson)

Major revisions were accomplished in the hydrodynamics routines in POOL to allow the compressible/incompressible algorithms to function better and to avoid fluctuations in neutronics predictions caused by the PIC (Particle-in-Cell) algorithms.

In particular, we have developed a new technique which we call (Distributed)-PIC (Particle-in-Cell). The concept is simple and its implementation was very effective. The assignment of a certain amount of mass to each particle and the calculation of mass per cell by simply adding the masses of all particles in each cell is responsible for a major fault of the PIC scheme, namely that the mass in each cell makes step function changes in value as particles enter or leave the cell. This causes the neutronic properties of the grid to vary significantly from time step to time step by

amounts which are large compared to the actual hydrodynamic motion induced variations. To solve this problem, we simply assign a volume to each particle and distribute the associated mass uniformly over that volume. Thus, as a particle nears a cell edge, the associated mass and energy convect continuously and smoothly from one cell to the next. This D-PIC technique has the advantages of PIC and appears to eliminate one major disadvantage.

A second modification we are currently examining in the POOL hydrodynamic algorithms is the decoupling of axial and radial motions for incompressible cells. While this introduces an obvious error, it does allow the calculations to proceed through the compressible/incompressible regions with no problems. Specifically, we have made the assumption that when a cell goes incompressible lump is accelerated axially and radially by the pressure gradients across it. As the incompressible region becomes more than one cell wide (radially) or high (axially), the radial momentum of the whole region is calculated and distributed radially so that each cell flux satisfies rU = constant. Similarly the axial momentum is redistributed over all axially contiguous incompressible cells such that U_z = constant. These cells are then treated as one large incompressible lump which is accelerated by the pressure gradient across it (in the same fashion that we treat the upper and lower sodium slugs as incompressible slugs in EPIC).

2. Bubble Collapse (Behrens) Effect (P. B. Abramson and T. A. Daly)

In attempting to calculate recriticality and the autocatalytic effects of bubble collapse induced streaming reduction, we have found that the current point kinetics options in FX2 are unstable for certain types of material motions. In particular, as a neutronic cell is voided of material and that material is pushed into adjacent cells, FX2 predicts reactivities which oscillate from positive to negative. Thus the point kinetics becomes unstable and the FX2 solution breaks down. We have investigated this effect both in FX2POOL and FX2-VENUS and find that it occurs with both. The shape step portion of the FX2 kinetics is initially able to correct the fluctuations, but since the amplitude grows from reactivity step to reactivity step, eventually the amplitude gets so large that the shape step calculation is unable to correct the problem. We are currently programming a global point kinetics scheme which when coupled with the shape steps will enable the stable prediction of the kinetics parameters. In addition, the global scheme has the potential advantage of significantly reduced neutronics computational time and core storage. The concept is as follows: The current points kinetics portions of FX2 use the cell by cell flux history to predict the cell's future flux and then use the flux to determine reactivity, etc. Since these local projections are unstable but the global behavior of the calculation is smooth, we are programming a point kinetics calculation which uses the normal FX2 path for the first few time steps (to build a global history) and then uses the past global reactivity history to project the future. This, as in the current FX2 version, is of course checked and updated by doing periodic shape calculations.

3. EPIC Development (P. A. Pizzica and P. B. Abramson)

Capability for cutting back the time step in EPIC in cases of over-compaction in the coolant channel (i.e., moving more material into a cell than it can physically hold) was added. Also the time-step is cut back whenever the local material velocity in a pin channel node violates one-fifth of the courant condition.

An option was added to allow an explicit calculation in time (instead of semi-implicit) after a specified real time point in the transient.

The number of particle-groups in the coolant channel was varied over as wide a range as possible (this number is dependent on the number of time steps since we currently require at least one particle-group generated per time step when there is any fuel ejection). Since there was little difference in the results, the number of particle-groups can now be reduced. In the future, some capability for combining groups in the channel will be added to reduce computer run time.

It was found necessary to trace the interface position for the forced convection of the fission gas in the channel because in the case of a partially voided channel an artificial convection would otherwise occur, which would smear the gas instantly over a node as soon as the gas moved into it forcing convection into the next mode on the next time step. This leads to excessive convection and a dependence on time-step which is undesirable.

The effect of spatial mesh size in EPIC was investigated for a 5 cm long clad rip by using one, two and four nodes. Differences in significant parameters of about 10% were found, indicating some sensitivity of the results to mesh size.

After giving some thought to a fuel vapor driven pin failure, we have decided that fuel vapor condensation is too ill defined an area to be able to treat analytically at this time. The net effect of fuel vapor condensation is to cause the liquid fuel temperature to decrease and the pressure in the vapor to decrease. The process of energy transfer from hot liquid fuel to cold liquid sodium may be thought of as being bounded by two extremums. One extremum is that energy is only exchanged from liquid to liquid, in which case the partial vapor pressures are the saturation pressures of the liquid. The other extremum is that energy is only exchanged by the vapors. In this latter case, the vapor of the hot liquid will be cooled to a pressure lower than the saturation pressure forcing generation of more vapor and thus drawing energy out of the hot liquid (with the corresponding inverse process going on for the other material). The real phenomenon falls somewhere between these extremes and depends upon geometry, material properties, etc. In EPIC, therefore, fuel vapor condensation will be treated by using a variable heat transfer rate between fuel (a relatively small amount of liquid fuel will be ejected into the channel in a fuel vapor voiding case) and liquid sodium to simulate variable condensation rates of fuel vapor and concurrent pressure designation.

Preparation of a data base to be used for extensive comparisons of EPIC and PLUTO and for an EPIC parameter study was begun. A paper presenting the EPIC code was prepared for the Chicago Meeting on Fast Reactor Safety in October.

4. KACHINA Conversion to IBM (J. Sienicki, T. A. Daly and P. B. Abramson)

The KACHINA code was converted from its original CDC version to IBM and is now running on the ANL IBM 370 model 195.

A basic problem in checking out our IBM version is the lack of available sample problems. We have been in contact with Jack Travis (LASL) who promised to generate some sample cases for us.

We will attempt to determine what are the capabilities of KACHINA and the techniques employed in it and if it can be adapted for use in POOL.

IV. COORDINATION OF RSR SAFETY RESEARCH

P. Abramson visited LASL on August 2 to discuss pin burst and possible sodium entrapment in the low power regions of a core undergoing LOF TOP with M. Stevenson and J. Jackson. The major question which needs to be resolved here is the amount of mixing between fuel and coolant in such circumstances. That mixing will be strongly influenced by the specific mode of clad failure as follows: if the clad fails in one continuous rip, the remaining clad could act as a radial barrier between fuel and coolant, providing resistance to heat transfer, but if the clad undergoes brittle shattering into many small pieces, the fuel to coolant heat transfer will be very strong. Thus, the mechanistics of clad failure under rapid (millisecond) loading up to pressures of order 100 atm need to be experimentally determined. The results will bear heavily upon whether or not significant work energy is obtained from coolant in an LOF TOP accident.

Abramson attended an Aerosol Release and Transport review group meeting at Oak Ridge on August 19 and 20 and submitted comments to M. Silberberg.

Abramson attended a two-day (September 13 and 14) SIMMER workshop at LASL to help BNL get ready to implement SIMMER for DPM, and then spent a day at SANDIA (September 15) reviewing the ACPR experimental results to date.

V. EVALUATION OF PROGRESS IN REACTOR SAFETY RESEARCH

Publications at the Fast Reactor Safety Meeting in Chicago

1. "Core Disruptive Accident and Recriticality Analysis with FX2POOL," by P. B. Abramson.

2. "EPIC" P. A. Pizzica and P. B. Abramson

Accepted for Publication in NSE and Final MS's Approved

1. "Basic Collapse Criteria for Boiling Fuel/Steel Mixtures," P. B. Abramson.

2. "FX2POOL - A Two-Dimensional Coupled Hydrodynamic Thermodynamic and Neutronic Computer Model for HCDA Analysis," P. B. Abramson.

MONTE CARLO ANALYSIS AND CRITICALS PROGRAM
PLANNING FOR SAFETY-RELATED CRITICALS
(A2018)

VI. MONTE CARLO ANALYSIS OF SAFETY-RELATED CRITICALS

To a large extent the VIM-S_n discrepancies, reported earlier[1], have been resolved. It now appears that these discrepancies were mainly due to:

1. statistical errors in the VIM results, and

2. inadequacies in the original TWOTRAN S_4-P_0 approximations.

During this last report period the VIM run has been continued, and a TWOTRAN S_4-P_1 has been run. In Table III new and old results, for the reference core, are compared.

TABLE III. Reference Core Eigenvalues

	Previously Reported	New Results
Differential Theory	1.000	-
VIM	0.998 ± 0.0025[a]	1.0045 ± 0.0010[a]
TWOTRAN (S_4-P_0)	1.010	
(S_4-P_1)		1.0093
(S_8-P_0)		1.0090

[a]Quoted uncertainties are standard deviations.

It will be seen, from data listed in this Table, that the new and old VIM results differ by about 2.2 times the standard deviations of the difference. The probability of such a change is $\sim$ 3%, a small but not negligible probability.

At this point no S_8-P_1 results are available: an S_8-P_1 has not been run because of the cost of such a computation. However, if we assume the $S_4 \rightarrow S_8$ and $P_0 \rightarrow P_1$ corrections to be additive we estimate an S_8-P_1 eigenvalues $\lambda_{S8\text{-}P1} = 1.0083$, an eigenvalue which differs from the latest VIM by slightly less than 0.4%. Although this discrepancy is still statistically significant, it is not nearly as serious as the original 1.2% discrepancy.

Latest results for the spherical model are listed in Table IV. It will be seen that the VIM λ is higher than the Sn λ by $\sim$ 0.5% in both the cylindrical and spherical calculations, in this sense the 2-D and 1-D results are now consistent.

TABLE IV. Spherical Model Eigenvalues
Best Available Results

Differential Theory	1.0040
VIM	1.0096 ± 0.0015
ANISN (S_8-P_1)	1.0113

VII. PLANNING OF DEMO SAFETY RELATED CRITICAL EXPERIMENTS

During this quarter the schedule for the Demo safety related critical experiments was fixed, and a preliminary plan for the experimental program, consistent with this schedule, was prepared. The preliminary program plan was reviewed at a meeting at NRC in Silver Springs on September 21, 1976. Some additional planning and analysis work is required as a result of suggestions made at the program review meeting. This work will be reported in the next quarterly report.

The safety related critical experiments are scheduled for the six month period from July 1, 1977 to December 31, 1977. The revised program plan consistent with this period is presented in Tables V and VI. Substantial deletions from the previous plan were, of course, necessary since the previous plan was based on a 1215 month period of critical experiments. Schedule estimates indicate that the revised plan can be completed in the available six-month period but no schedule contingency is included. It is recommended that some phases of the experimental program be assigned a lower priority and be considered candidates for deletion if the program is running behind schedule. This decision would be made during the course of the measurements when progress on the schedule is known.

The program outlined in the program plan is divided into five major phases. They are:

1. Reference core.
2. Sodium-Voided Configurations.
3. Fuel-Slump-Out Configurations.
4. Fuel-Slump-In Configurations.
5. Blanket Collapse Configurations (with Fuel-Slump-In).

These are the configurations outlined in Tables V and VI, and they are shown in Fig. 7. The Fuel-Slump-Out core is divided into two major configurations. Note that the origin in each of the drawings on this figure is the core center. The core height is 2H, 92.4 cm, and the H/D = 1.0.

TABLE V. Sequence of Critical Assembly Core Configurations for Safety-Related Critical Experiments

Phase	Step	Measurements at Critical (See Table II)
I. Reference Core.	A. Reference Case.	Yes
II. Sodium-Voided Configurations.	A. Sodium Voiding in Central 37 Drawers (r = 18.96 cm).	
a. Core Loading Adjusted so that all Steps Subcritical Except as Noted.	1. Void Upper Axial Blanket.	
	2. Void Full Height of Core and Blankets.	
III. Fuel-Slump-Out Configurations.	A. Fuel Slump Out in Central 37 Drawers. All Fuel in Region for Z = 0 to Z = H/2 Slumps into Region H/2 to H, Where H is the Half Height of Core and Z = 0 is at the Core Midplane.	
a. All Measurements Made with Central 37 Drawers Na-Voided.	1. Slump Upper Half of Core.	
b. Core Loading Adjusted so that all Steps Subcritical Except as Noted.	2. Slump Over Full Core Height.	Yes
	3. Adjust Case C(2) to Critical.	
	4. Start From Step A(2). Unslump Fuel in Bottom Half of Core.	
	B. Move Slumpled-Fuel Regions into Axial Blankets.	
	1. Upper Half of Core (With Bottom Half Unslumped).	
	2. Full Core Height.	
	3. Adjust B(2) to Critical.	Yes
IV. Fuel-Slump-In Configurations.	A. Fuel Slump In in Central 37 Drawers. All Fuel in Region Z = H to Z = H/2 Slumps into Region Z = H/2 to Z = 0, Where H is the Half Height of the Core and Z = 0 is at the Core Midplane.	
a. All Measurements With Central 37 Drawers Na-Voided.		

TABLE V (contd.)

	Phase		Step	Measurements at Critical (See Table II)
	b. Core Loading Adjusted so that all Steps Subcritical Except as Noted.	1.	Establish New Sodium-Voided Reference.	
		2.	Slump in Upper Half of Core.	
		3.	Slump Over Full Core Height.	
		4.	Adjust case A(2) to Critical.	Yes
		5.	Start From Step A(3). Unslump Bottom Half of Core.	
V.	Blanket Collapse Configurations.	A.	Start From Step IV A(5). Fuel Slumped in Top Half of Core and Unslumped in Bottom Half of Core.	
	a. All Measurements With Central 37 Drawers Na-Voided.	1.	Collapse Upper Axial Blanket Material so that it is Directly on Top of Slumped-In Core Material.	
	b. Core Loading Adjusted so that all Steps Subcritical Except as Noted.	2.	Adjust Step A(1) to Critical.	Yes

TABLE VI. Outline of Measurements for Safety-Related Critical Experiments

Phase/Step (See Table I)	k_{eff}	Spectrum	Reaction Rate Profiles[a]	Material Worths[b]	Doppler Coefficient
I A (Ref. Core)	✓	Core Center	Axial and Radial	Fuel and Structure — Axial Profiles	Core Center
III A(3) (Fuel-Slump-Out, 1)	✓		Axial and Radial	Axial Profiles	
III B(3) (Fuel-Slump-Out, 2)	✓		Axial and Radial	Axial Profiles	
IV A(4) (Fuel-Slump-In, 1)	✓	Core Center	Axial and Radial	Axial Profiles	Core Center
V A (2) (Blanket Collapse)	✓		Axial and Radial	Axial Profiles	

[a] Reaction rates will include $^{239}Pu(n,f)$, $^{238}U(n,f)$ and $^{238}U(n,\gamma)$. In some cases $^{235}U(n,f)$ may be substituted for $^{239}Pu(n,f)$. The detailed arrangement of the foils must be coordinated with the Monte Carlo validation work to insure that the experimental arrangements are calculable.

[b] Axial worth profiles will be made for ^{239}Pu, ^{238}U and SS. Central worths may be obtained for several other materials (e. g., Na, ^{10}B).

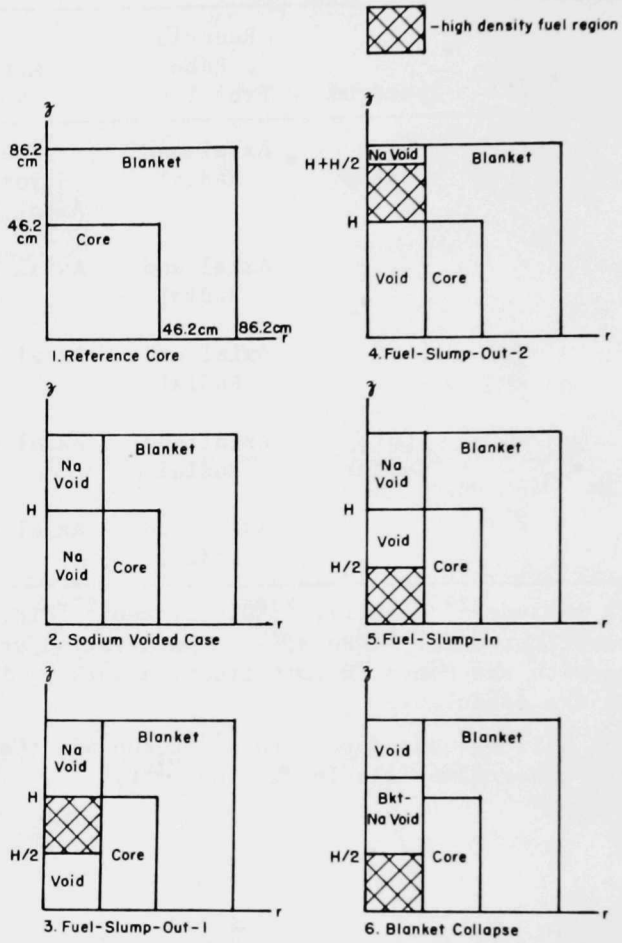

Fig. 7. RSR Safety Related Critical Experiments, Core Configurations. (Note: Core Height is 2H, 92.4 cm.)

Preanalysis on these configurations is resuming. Four particular areas will be analyzed initially.

1. Calculations will be made of the Fuel-Slump-Out configuration. To date only Fuel-Slump-In cores have been analyzed.

2. Calculations will be made with the fuel slumping in only one axial half of the core. This analysis will allow us to investigate some axially asymmetric cases.

3. Various fuel densities in the fuel-slump regions will be evaluated.

4. The volume of the fuel-slump regions will be varied in a way that fuel is not conserved within the assembly. It was decided at the review meeting that varying the volume of the fuel-slump region was the preferred method of adjusting system reactivity. These calculations will evaluate the potential of this method.

VIII. FINITE DIFFERENCING IN 2 3-D STAGGERED MESH SUITABLE FOR IRREGULAR BOUNDARY APPLICATIONS

(W. T. Sha, H. M. Domanus and R. C. Schmitt)

A. Introduction

A formulation utilizing a finite difference scheme for a direct numerical simulation of time varying two-phase flow problems in three space dimensions with irregular boundary geometry is presented. The formulation of such problems introduces a complicated set of coupled non-linear partial differential equations for the conservation of mass, momentum, energy, appropriate constitutive equations coupling the two phases. Discretization of the partial differential equations by finite difference procedures allow for numerical solution of the governing equations. The finite difference scheme uses a staggered grid system so often used in hydrodynamics where the velocities are located at the tips of a cell with the pressure, temperature, and density being located at the central mesh point as shown in Fig. 8. Although this staggered mesh provides several conservation properties it requires some adjustment when dealing with irregular boundaries.

If the boundaries were curved and the variables were discretized at every mesh point the usual formulation as described in any textbook on numerical solution of partial differential equations could be utilized. However, the staggered mesh requires that only certain boundary intersections of the mesh system be allowed. At this time it is required that in any given direction for a boundary intersection the first internal mesh point always be a pressure point. Because of the usual sensitivity involved in pressure calculations the polated to the wall. In the last section of this memo the extrapolation procedure is defined. For example, for a no-slip boundary condition, the conditions on velocity on the wall require that all of the components be indentically zero. However, in the case of a free-slip wall where the tangential velocity is non-zero and parallel to the streamline, only the normal component is zero. Hence, from a correct calculation of the internal velocities due to internal pressure gradients the velocities or their averages can be extrapolated to the wall and the proper tangential velocity

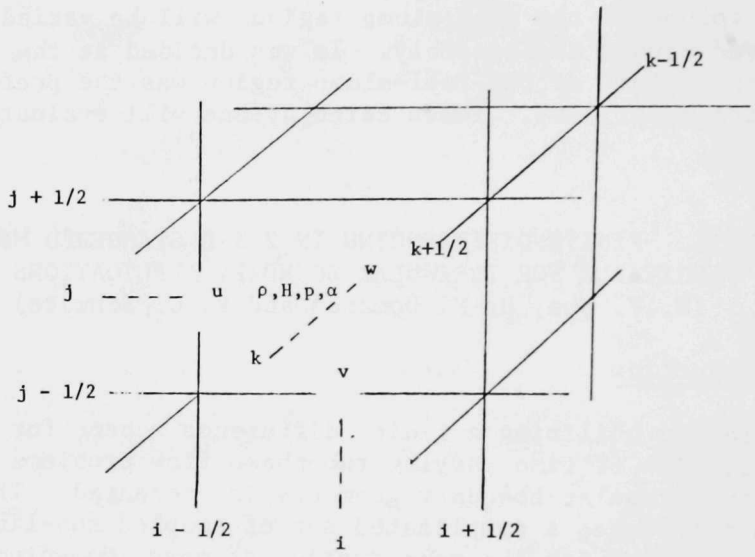

ρ,H,p,α = density, enthalpy, pressure, void fraction

u,v,w = velocity components in x,y,z

Fig. 8. Location of Variables and Indices About a Computational Cell (Staggered Mesh Systems).

obtained along the wall. Although the requirement for the first internal mesh point to be a pressure point is presently being incorporated, other boundary-mesh cuts will be investigated to determine if this restriction can be alleviated.

B. Finite Differencing of the Governing Differential Equations

In order to obtain estimates of the dependent variable distributions at discrete points throughout the domain of interest, partial derivative expressions appearing in the governing differential equations are approximated by finite differences. Location of these descrete points is made via a staggered mesh partitioning of the solution domain. The staggered mesh partitioning consists of four different mesh systems. One mesh system for the field variables (i.e., ρ, P, α, H) and one for each of the three velocity components (u, v, w).

To illustrate the finite difference techniques as applied to a staggered mesh, governing equations 1-5 will be considered. While these equations contain other terms (i.e., O.T.), only the convective terms will be considered here.

$$\frac{\partial(\alpha_\ell \rho_\ell)}{\partial t} + \frac{\partial}{\partial x}(\alpha_\ell \rho_\ell u_\ell) + \frac{\partial}{\partial y}(\alpha_\ell \rho_\ell v_\ell) + \frac{\partial}{\partial z}(\alpha_\ell \rho_\ell w_\ell) = \text{O.T.} \tag{1}$$

$$\frac{\partial(\alpha_\ell \rho_\ell u_\ell)}{\partial t} + \frac{\partial}{\partial x}(\alpha_\ell \rho_\ell u_\ell u_\ell) + \frac{\partial}{\partial y}(\alpha_\ell \rho_\ell u_\ell v_\ell) + \frac{\partial}{\partial z}(\alpha_\ell \rho_\ell u_\ell w_\ell) = -\alpha_\ell \frac{\partial P}{\partial x} + \text{O.T.} \tag{2}$$

$$\frac{\partial(\alpha_\ell \rho_\ell v_\ell)}{\partial t} + \frac{\partial}{\partial x}(\alpha_\ell \rho_\ell v_\ell u_\ell) + \frac{\partial}{\partial y}(\alpha_\ell \rho_\ell v_\ell v_\ell) + \frac{\partial}{\partial z}(\alpha_\ell \rho_\ell v_\ell w_\ell) = -\alpha_\ell \frac{\partial P}{\partial y} + \text{O.T.} \tag{3}$$

$$\frac{\partial(\alpha_\ell \rho_\ell w_\ell)}{\partial t} + \frac{\partial}{\partial x}(\alpha_\ell \rho_\ell w_\ell u_\ell) + \frac{\partial}{\partial y}(\alpha_\ell \rho_\ell w_\ell v_\ell) + \frac{\partial}{\partial z}(\alpha_\ell \rho_\ell w_\ell w_\ell) = -\alpha_\ell \frac{\partial P}{\partial z} + \text{O.T.} \tag{4}$$

$$\frac{\partial(\alpha_\ell \rho_\ell H_\ell)}{\partial t} + \frac{\partial(\alpha_\ell \rho_\ell H_\ell u_\ell)}{\partial x} + \frac{\partial(\alpha_\ell \rho_\ell H_\ell v_\ell)}{\partial y} + \frac{\partial(\alpha_\ell \rho_\ell H_\ell w_\ell)}{\partial z} = \frac{\partial}{\partial t}(\alpha_\ell P) + \frac{\partial}{\partial x}(\alpha_\ell P u_\ell)$$

$$+ \frac{\partial}{\partial y}(\alpha_\ell P v_\ell) + \frac{\partial}{\partial z}(\alpha_\ell P w_\ell) - \alpha_\ell P\left[\frac{\partial u_\ell}{\partial x} + \frac{\partial v_\ell}{\partial y} + \frac{\partial w_\ell}{\partial z}\right] + \text{O.T.} \tag{5}$$

The finite differencing of these equations will be general enough to accomodate an irregularly shaped domain.

To clarify locations on the staggered mesh, reference is made to field points, u points, v points, and w points. Equation 1 and 5 are at field points while equations 2, 3, and 4 are at u points, v points, and w points, respectively.

Consider equation 1, term by term, evaluated at field point 0 in Figs. 9 and 10.

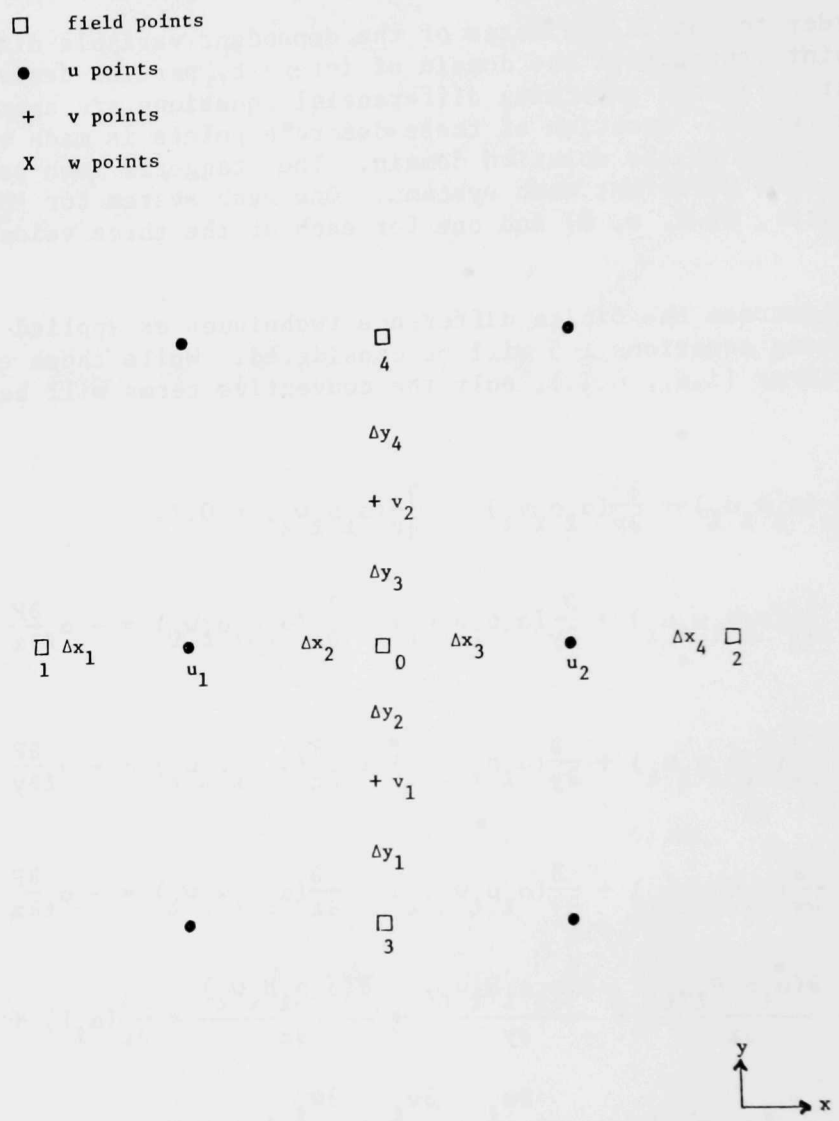

Fig. 9. Grid System Around Field Point '0' in x-y Plane.

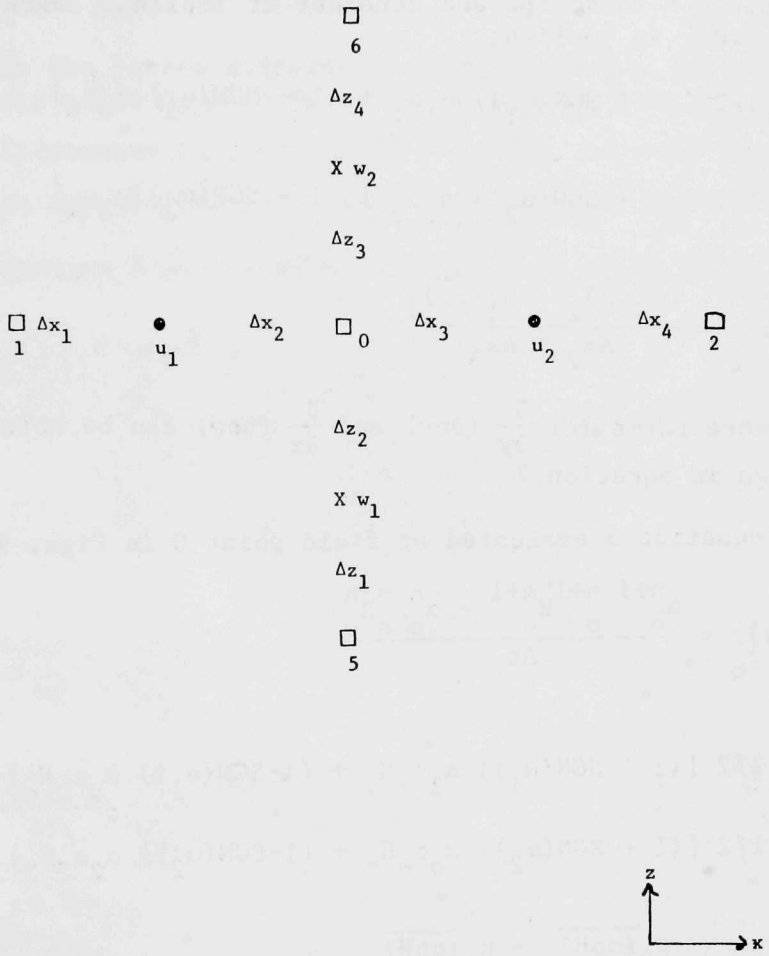

Fig. 10. Grid System Around Field Point '0' in x-z Plane.

$$\frac{\partial}{\partial t}(\alpha_\ell \rho_\ell)\Big|_o = \frac{(\alpha_\ell)_o^{n+1}(\rho_\ell)_o^{n+1} - (\alpha_\ell)_o^{n}(\rho_\ell)_o^{n}}{\Delta t} \tag{6}$$

Hereafter, delete ℓ subscript and consider it implied. When superscript n is absent consider it implied.

Let $\overline{(\alpha\rho)}_1 = 1/2\ [(1 + SGN(u_1))\ \alpha_1\rho_1 + (1 - SGN(u_1))\alpha_o\rho_o]$

$$\overline{(\alpha\rho)}_2 = 1/2\ [(1 + SGN(u_2))\ \alpha_o\rho_o + (1 - SGN(u_2))\alpha_2\rho_2]$$

$$\frac{\partial}{\partial x}(\alpha\rho u)\Big|_o = \frac{u_2\overline{(\alpha\rho)}_2 - u_1\overline{(\alpha\rho)}_1}{\Delta x_2 + \Delta x_3} \tag{7}$$

Finite difference forms for $\frac{\partial}{\partial y}(\partial\rho v)$ and $\frac{\partial}{\partial z}(\partial\rho w)$ can be obtained in similar manner as shown in equation 7.

Consider equation 5 evaluated at field point 0 in Figs. 9 and 10.

$$\frac{\partial}{\partial t}(\alpha\rho H)\Big|_o = \frac{\alpha_o^{n+1}\rho_o^{n+1}H_o^{n+1} - \alpha_o^{n}\rho_o^{n}H_o^{n}}{\Delta t} \tag{8}$$

Let $\overline{(\alpha\rho H)}_1 = 1/2\ [(1 + SGN(u_1))\ \alpha_1\rho_1H_1 + (1-SGN(u_1))\ \alpha_o\rho_oH_o]$

$$\overline{(\alpha\rho H)}_2 = 1/2\ [(1 + SGN(u_2))\ \alpha_o\rho_oH_o + (1-SGN(u_2))\ \alpha_2\rho_2H_2]$$

$$\frac{\partial}{\partial x}(\alpha\rho Hu)\Big|_o = \frac{u_2\overline{(\alpha\rho H)}_2 - u_1\overline{(\alpha\rho H)}_1}{\Delta x_2 + \Delta x_3} \tag{9}$$

Finite difference forms for $\frac{\partial}{\partial y}(\partial\rho Hv)$ and $\frac{\partial}{\partial t}(\partial\rho Hw)$ can be obtained in similar manner as shown in equation 9.

Let $\overline{(\alpha P)}_1 = 1/2\ [(1 + SGN(u_1))\ \alpha_1P_1 + (1 - SGN(u_1))\ \alpha_oP_o]$

$$\overline{(\alpha P)}_2 = 1/2\ [(1 + SGN(u_2))\ \alpha_oP_o + (1 - SGN(u_2))\ \alpha_2P_2]$$

$$\frac{\partial}{\partial x}(\alpha Pu)\Big|_o = \frac{u_2\overline{(\alpha P)}_2 - u_1\overline{(\alpha P)}_1}{\Delta x_2 + \Delta x_3} \tag{10}$$

Finite difference forms for $\frac{\partial}{\partial y}(\partial\rho v)$ and $\frac{\partial}{\partial z}(\partial\rho w)$ can be obtained in similar manner as shown in equation 10.

$$\alpha P \frac{\partial u}{\partial x}\Big|_o = \alpha_o P_o \frac{u_2 - u_1}{\Delta x_2 + \Delta x_3} \tag{11}$$

Finite difference forms for $\partial P \frac{\partial v}{\partial y}$ and $\partial P \frac{\partial w}{\partial z}$ can be obtained in similar manner as shown in equation 11.

Note that in the finite difference expressions from equations 1 and 5 as evaluated at field point 0, only Δx_2, Δx_3, Δy_2, Δy_3, Δz_2, and Δz_3 appear. However, other increments Δx_1, Δx_4, Δy_1, Δy_4, Δz_1, Δz_4 will appear in the finite difference expressions of diffusive terms which are included in O.T.

Consider equation 2 evaluated at u-point 0 in Figs. 11 and 12.

Let

$$\overline{(\alpha\rho)}_o^n = \frac{\Delta x_3 \alpha_3^n \rho_3^n + \Delta x_4 \alpha_2^n \rho_2^n}{\Delta x_3 + \Delta x_4} \tag{12}$$

$$\frac{\partial}{\partial t}(\alpha\rho u)\Big|_o = \frac{\overline{(\alpha\rho)}_o^{n+1} u_o^{n+1} - \overline{(\alpha\rho)}_o^n u_o^n}{\Delta t}$$

Let $\overline{(\alpha\rho)}_1 = \dfrac{\Delta x_1 \alpha_2 \rho_2 + \Delta x_2 \alpha_1 \rho_1}{\Delta x_1 + \Delta x_2}$

$$\overline{(\alpha\rho)}_2 = \frac{\Delta x_5 \alpha_4 \rho_4 + \Delta x_6 \alpha_3 \rho_3}{\Delta x_5 + \Delta x_6}$$

$$\bar{u}_1 = \frac{\Delta x_2 u_o + \Delta x_3 u_1}{\Delta x_2 + \Delta x_3}$$

$$\bar{u}_2 = \frac{\Delta x_4 u_2 + \Delta x_5 u_o}{\Delta x_4 + \Delta x_5}$$

$$\overline{\overline{(\alpha\rho u)}}_1 = \frac{1}{2}\left[(1 + \mathrm{SGN}\ (\bar{u}_1))\ \overline{(\alpha\rho)}_1 u_1 + (1 - \mathrm{SGN}\ (\bar{u}_1))\ \overline{(\alpha\rho)}_o u_o\right]$$

$$\overline{\overline{(\alpha\rho u)}}_2 = \frac{1}{2}\left[(1 + \mathrm{SGN}\ (\bar{u}_2))\ \overline{(\alpha\rho)}_o u_o + (1 - \mathrm{SGN}\ (\bar{u}_2))\ \overline{(\alpha\rho)}_2 u_2\right]$$

$$\frac{\partial}{\partial x}(\alpha\rho uu)\Big|_o = \frac{\bar{u}_2 \overline{\overline{(\alpha\rho u)}}_2 - \bar{u}_1 \overline{\overline{(\alpha\rho u)}}_1}{\Delta x_3 + \Delta x_4} \tag{13}$$

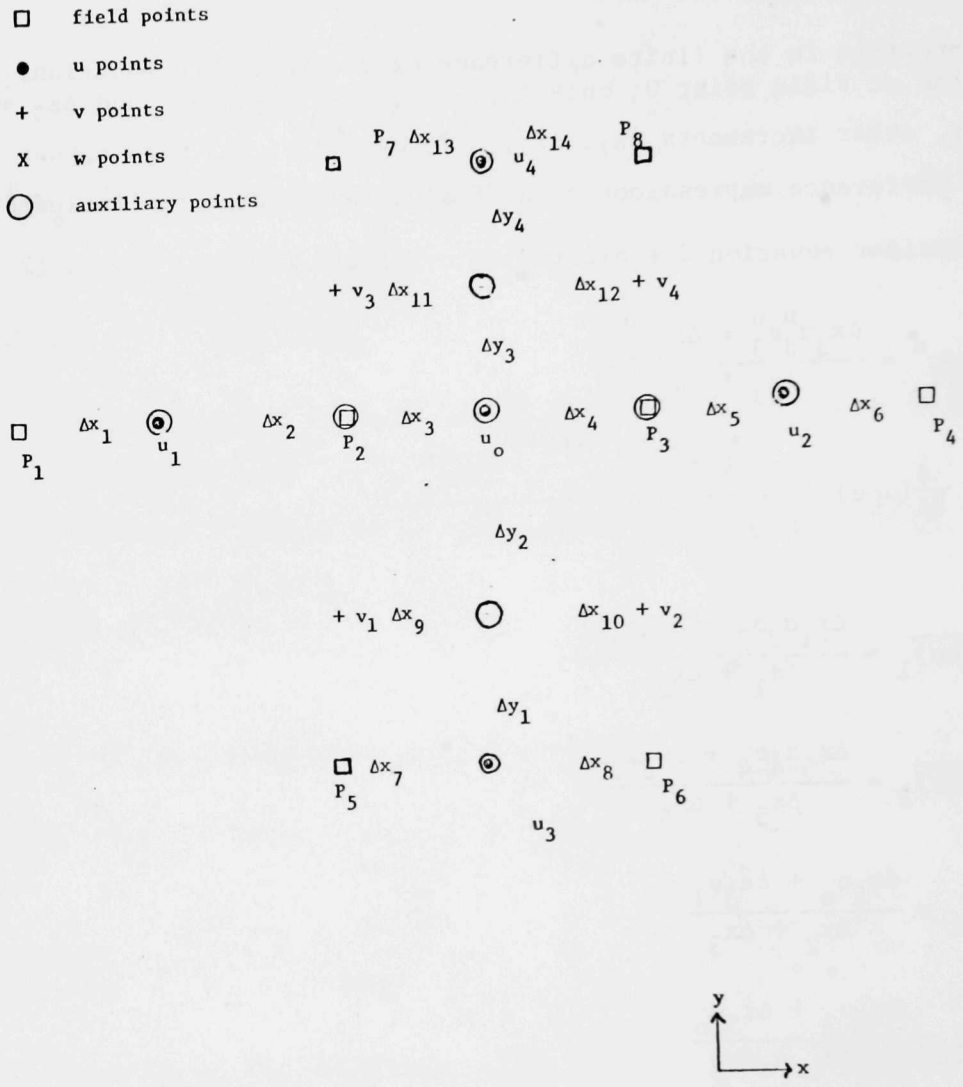

Fig. 11. Grid System Around u-Point '0' in x-y Plane.

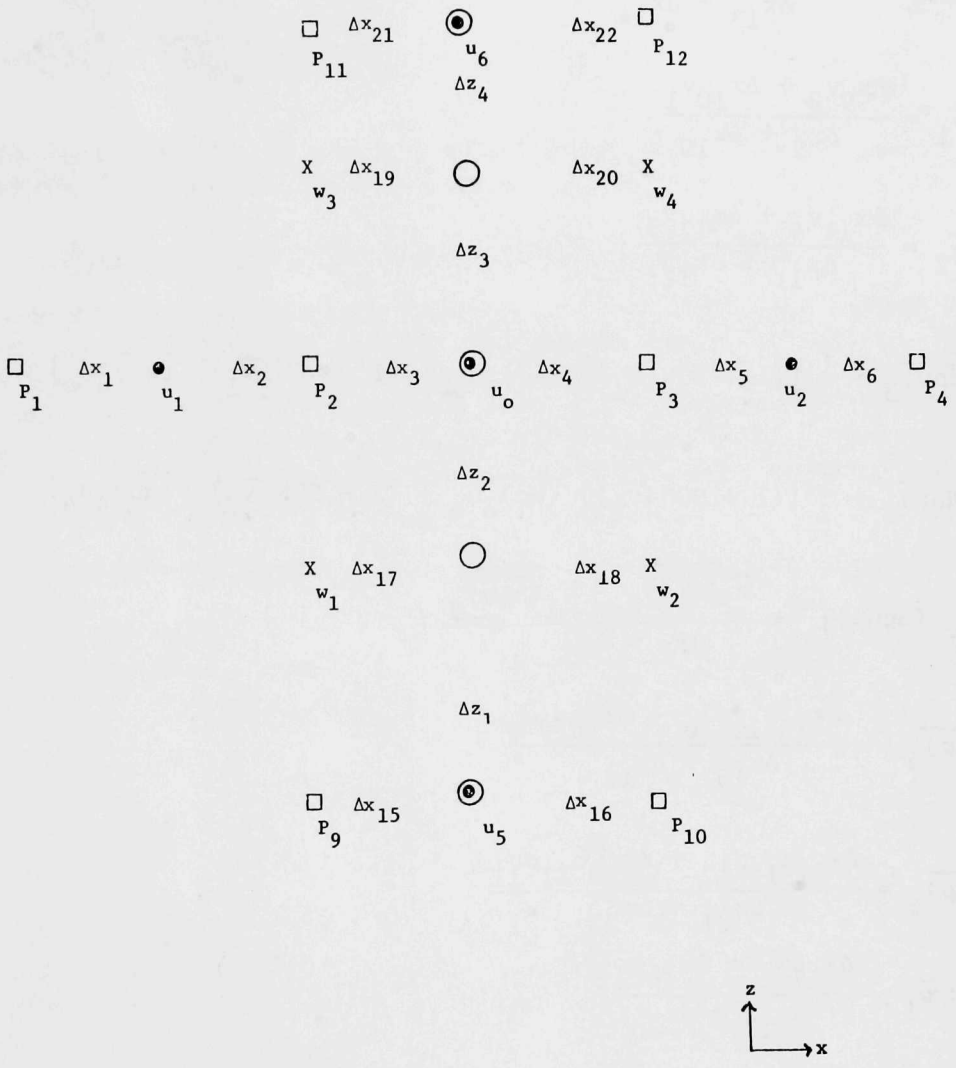

Fig. 12. Grid System Around u-Point '0' in x-z Plane.

Let $\overline{(\alpha\rho)}_3 = \dfrac{\Delta x_7 \alpha_6 \rho_6 + \Delta x_8 \alpha_5 \rho_5}{\Delta x_7 + \Delta x_8}$

$$\overline{(\alpha\rho)}_4 = \frac{\Delta x_{13} \alpha_8 \rho_8 + \Delta x_{14} \alpha_7 \rho_7}{\Delta x_{13} + \Delta x_{14}}$$

$$\bar{v}_1 = \frac{\Delta x_9 v_2 + \Delta x_{10} v_1}{\Delta x_9 + \Delta x_{10}}$$

$$\bar{v}_2 = \frac{\Delta x_{11} v_4 + \Delta x_{12} v_3}{\Delta x_{11} + \Delta x_{12}}$$

$$\overline{\overline{(\alpha\rho u)}}_3 = \frac{1}{2}\left[(1 + \mathrm{SGN}(\bar{v}_1))\ \overline{(\alpha\rho)}_3 u_3 + (1 - \mathrm{SGN}(\bar{v}_1))\ \overline{(\alpha\rho)}_o u_o\right]$$

$$\overline{\overline{(\alpha\rho u)}}_4 + \frac{1}{2}\left[(1 + \mathrm{SGN}(\bar{v}_2))\ \overline{(\alpha\rho)}_o u_o + (1 - \mathrm{SGN}(\bar{v}_2))\ \overline{(\alpha\rho)}_4 u_4\right]$$

$$\frac{\partial}{\partial y}\,(\alpha\rho uv)\Big|_o = \frac{\bar{v}_2 \overline{\overline{(\alpha\rho u)}}_4 - \bar{v}_1 \overline{\overline{(\alpha\rho u)}}_3}{\Delta y_2 + \Delta y_3} \qquad (14)$$

Let $\overline{(\alpha\rho)}_5 = \dfrac{\Delta x_{15} \alpha_{10} \rho_{10} + \Delta x_{16} \alpha_9 \rho_9}{\Delta x_{15} + \Delta x_{16}}$

$$\overline{(\alpha\rho)}_6 = \frac{\Delta x_{21} \alpha_{12} \rho_{12} + \Delta x_{22} \alpha_{11} \rho_{11}}{\Delta x_{21} + \Delta x_{22}}$$

$$\bar{w}_1 = \frac{\Delta x_{17} w_2 + \Delta x_{16} w_1}{\Delta x_{17} + \Delta x_{16}}$$

$$\bar{w}_2 = \frac{\Delta x_{19} w_4 + \Delta x_{20} w_3}{\Delta x_{19} + \Delta x_{20}}$$

$$\overline{\overline{(\alpha\rho u)}}_5 = \frac{1}{2}\left[(1 + \mathrm{SGN}\ (\bar{w}_1))\ \overline{(\alpha\rho)}_5\ u_5 + (1 - \mathrm{SGN}\ (\bar{w}_1))\ \overline{(\alpha\rho)}_o u_o\right]$$

$$\overline{\overline{(\alpha\rho u)}}_6 = \frac{1}{2}\left[(1 + \mathrm{SGN}\ (\bar{w}_2))\ \overline{(\alpha\rho)}_o\ u_o + (1 - \mathrm{SGN}\ (\bar{w}_2))\ \overline{(\alpha\rho)}_6 u_6\right]$$

$$\frac{\partial}{\partial z}\,(\alpha\rho uw)\Big|_o = \frac{\bar{w}_2 \overline{\overline{(\alpha\rho u)}}_6 - \bar{w}_1 \overline{\overline{(\alpha\rho u)}}_5}{\Delta z_2 + \Delta z_3} \qquad (15)$$

Let $\overline{(\alpha)}_o = \dfrac{\Delta x_3 \alpha_3 + \Delta x_4 \alpha_2}{\Delta x_3 + \Delta x_4}$

$$(\alpha \frac{\partial P}{\partial x})\Big|_o = \overline{(\alpha)}_o \left[\frac{P_3 - P_2}{\Delta x_3 + \Delta x_4} \right] \qquad (16)$$

The finite difference forms for the terms in Equation 3 and 4 can be obtained in similar manner as shown in Equations 12 to 16.

C. Extrapolation Procedure for Irregular Boundaries

In problems where the region under consideration has a curved boundary, it is necessary to determine certain variables through the use of irregular cells. A method for determining a variable located on a boundary from internally calculated points is presented. The method uses an interpolation technique which eliminates the need for information from points external to the boundary , which are in fact purely fictitious and inadmissible with respect to the finite difference scheme.

Suppose a general function f is known at point x_o and x_{+1} and designated by $f_{i,j,k}$ and $f_{i+1,j,k}$ respectively, as shown in Fig 13. If the boundary passes through point x, then $f_{i-1,j,k}$ located at x_{-1} is exterior to the boundary and sould not be used in the determination of $f_{i,j,k}$ at point x.

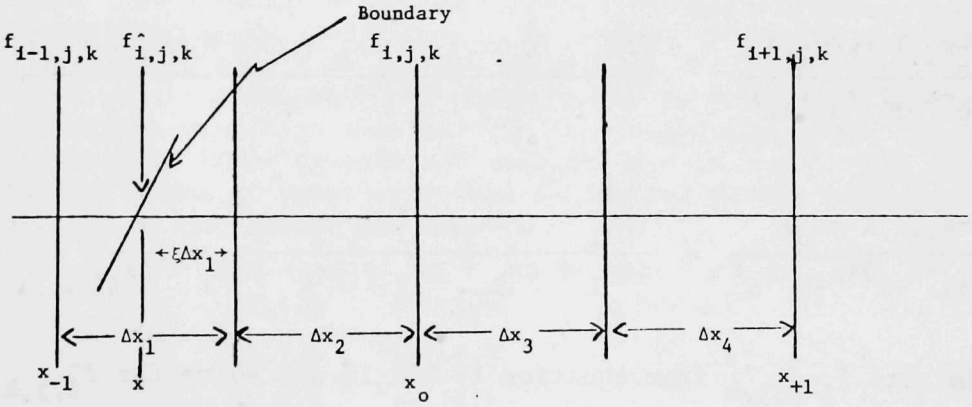

Fig. 13 Typical Curved Boundary Intersect with Rectangular Mesh System.

It is noted that equation 17 requires information at point x_{-1} for $f_{i-1,j,k}$. A second approximation must be made for $f_{i,j,k}$ which can eliminate $f_{i-1,j,k}$. If a three point Lagrangian interpolation is used for points x_{-1}, x_o and x_{+1}, elimination of $f_{i-1,j,k,}$ can be accomplished. A value for $f\hat{}_{i,j,k}$ can be obtained as follows through Lagrangian interpolation.

As a first approximation to the value $f_{\hat{i},j,k}$ on the boundary, a linear interpolation involving the information at points x_o and x_{-1} is made.

$$f_{i,j,k} = \frac{\Delta x_1(1 - \xi)\, f_{i,j,k} + (\xi\, \Delta x_1 + \Delta x_2)\, f_{i-1,j,k}}{\Delta x_2 + \Delta x_1}$$

$$= A_1\, f_{i,j,k} + A_2\, f_{i-1,j,k}$$

where $$A_1 = \frac{(1 - \xi)\, \Delta x_1}{\Delta x_2 + \Delta x_1}$$

$$A_2 = \frac{\xi\, \Delta x_1 + \Delta x_2}{\Delta x_2 + \Delta x_1} \qquad (17)$$

$$f_{\hat{i},j,k} = L_o\, f_{i-1,j,k} + L_i\, f_{i,j,k} + L_2\, f_{i+1,j,k} \qquad (18)$$

where L_o, L_1 and L_2 are the Lagrangian coefficients given by

$$L_o = \frac{(x-x_o)\,(x-x_{+1})}{(x_{-1}-x_o)\,(x_{-1}-x_{+1})} = \frac{(\xi\, \Delta x_1 + \Delta x_2)\,(\xi\, \Delta x_1 + \Delta x_2 + \Delta x_3 + \Delta x_4)}{(\Delta x_1 + \Delta x_2)\,(\Delta x_1 + \Delta x_2 + \Delta x_3 + \Delta x_4)}$$

$$L_1 = \frac{(x-x_{-1})\,(x-x_{+1})}{(x_o-x_{-1})(x_o-x_{+1})} = \frac{(\Delta x_1 - \xi\, \Delta x_1)\,(\xi\, \Delta x_1 + \Delta x_2 + \Delta x_3 + \Delta x_4)}{(\Delta x_1 + \Delta x_2)\,(\Delta x_3 + \Delta x_4)}$$

$$L_2 = \frac{(x-x_{-1})\,(x-x_o)}{(x_{+1}-x_{-1})(x_{+1}-x_o)} = \frac{(\Delta x_1 - \xi\, \Delta x_1)\,(\xi \Delta x_1 + \Delta x_2)}{(\Delta x_1 + \Delta x_2 + \Delta x_3 + \Delta x_4)\,(\Delta x_3 + \Delta x_4)}$$

Now eliminate $f_{i-1,j,k}$ from equation 17 and 18 and solve for $f_{\hat{i},j,k}$ on the boundary

$$f_{\hat{i},j,k} = \frac{1}{\left[1 - \frac{L_o}{A_2}\right]} \left\{ \left[L_1 - L_o\, \frac{A_1}{A_2} \right] f_{i,j,k} + L_2\, f_{i+1,j,k} \right\} \qquad (19)$$

Equation 19 allows for the determination of a variable on the boundary from determined interior field information.

D. Boundary Conditions

General geometrical configurations require the specification of several types of boundary conditions. The boundary conditions applied at the walls of the computing mesh are typically on the following: i) inflow, ii) outflow, iii) no-slip and iv) free slip. The boundary conditions are set before and after each interation. The treatment of specific boundary conditions because of staggered mesh in three dimensions always requires successive interpolation and extrapolation to provide the appropiate variables at the boundary.

The code as being developed will identify each boundary point separately and be named independent of the mesh indices. In addition, its location relative to the mesh layout will also be determined. For each named boundary point the unit vectors for the surface passing through the point will be determined and stored. This is done initially once and for all.

i) Inflow: For every intersection of an inflow surface by a u, v, or w velocity line, a vector velocity as well as density and enthalpy will be prescribed. Hence, if the point, for example, is labeled as point xx, then

$$u(xx) = u_b$$
$$v(xx) = v_b$$
$$w(xx) = w_b$$
$$\rho(xx) = \rho_b$$
$$h(xx) = h_b \text{ where } u_b,\ v_b$$

where u_b, v_b, w_b, ρ_b and h_b are specified.

ii) Outflow: On an outflow boundary several boundary conditions can be applied. Selection of the conditions to be used on an outflow boundary requires care. The conditions should be determined in such a way that their choice has minimal effect on the flow region of interest yet be physically meaningful. The idea of suing a condition that has the least upstream effect has been used successfully by many investigators and will be used in the present code. The codition is really one of smoothness that is applied to the velocity components. One possible set of conditions may be

$$u_{i,j,k} = u_{i-1,j,k}$$
$$v_{i,j,k} = v_{i-1,j,k}$$
$$w_{i,j,k} = w_{i-1,j,k}$$
$$\rho_{i,j,k} = \rho_{i-1,j,k},$$
$$h_{i,j,k,} = h_{i-1,j,k}$$

Other plausible conditions, such as the second derivative of the velocity components vanish may be used; however, the above are sufficient for illustrative purpose.

iii) No-Slip: The boundary conditions for a solid wall with viscosity present in the fluid require the sticking condition, i.e., no relative motion between the fluid particles at the wall and the wall. This condition implies

that the velocity components at the wall vanish. Since the boundary points are labeled we would have at point xx on the boundary

$$u_b(xx) = o$$
$$v_b(xx) = o$$
$$w_b(xx) = o$$

iv) Free Slip: The free-slip boundary condition for solid walls requires that there be zero normal flow across the wall, i.e., $\underline{V} \cdot \underline{n} = o$ where $\underline{n}$ is the unit normal to the surface. The unit vectors defining the boundary surface are calculated and stored at the start of the code. Hence, the velocity conditions which are appropriately interpolated and then extrapolated to a boundary point can be used to satisfy the zero normal flux condition as well as determine the tangential component, i.e., the slip velocity along the wall, by using the unit normal and decomposing the velocity.

For the cases (iii) and (iv) the temperature can be specified for either the constant wall temperature condition or the constant heat flux condition, whichever is appropriate for the given problem.

REFERENCES

1. *Preliminary Safety Analysis Report,* Clinch River Breeder Reactor Project, Section 4.4, Project Management Corp., Oak Ridge Tennessee.

2. D. C. Albright and R. A. Bari, *"Primary Pipe Rupture Accident Analysis for the Clinch River Breeder Reactor,"* BNL-NUREG-21656, Informal Report, Brookhaven National Laboratory (April, 1976).

3. H. H. Hummel and Kalimullah, *"Pipe Rupture Studies for the CRBR using DEMO and SAS"*, presented at the International Meeting on Fast Reactor Safety and Related Physics, Chicago, IL, (October 5-8, 1976)

4. M. G. Stevenson et al., *"Current Status and Experimental Basis of the SAS LMFBR Accident Analysis Code"*, Proceedings of the Fast Reactor Safety Meeting April 2-4, 1974, Beverly Hills, California, Conf-740401-P3, p. 1303.

5. D. A. Meneley et al, *"A Kinetics Model for Fast Reactor Analysis in Two Dimensions,"* Symposium on Dynamics of Nuclear Systems, University of Arizona Press, Tuscon, Arizona (March 23-25, 1972).

6. W. R. Bohl, private communication.

7. *Physics of Reactor Safety, Quarterly Report,* January-March 1976, ANL-76-72, p.8.

8. *Preliminary Safety Analysis Report,* Clinch River Breeder Reactor Project, Project Management Cooporation, Oak Ridge, Tennassee.

9. B. J. Toppel and H. Henryson II, *"Methodology and Applications of the MC^2-2/SDX Cross-Section Capability"*, Trans. Am. Nucl. Soc., *16*, 176, (1973).